Lauri Vähä-Savo, Clemens Icheln, Xiaoshu Lü, Antonio Palermo, Alessandro Marzani, and Katsuyuki Haneda

Antenna-Embedded Building Elements as Futuristic Cellular Infrastructure

Introduction to a multiphysics study.

A futuristic concept of antenna-embedded building elements is introduced. Such building elements aim at improving transmission coefficients of an incident electromagnetic wave for enhanced outdoor-to-indoor cellular communication, particularly in energy-efficient buildings. A challenge in designing antenna-embedded building elements is the need for a multiphysical study to ensure that embedding antennas do not deteriorate the original performance of building elements. Taking back-to-back passive spiral antenna systems embedded into a load-bearing wall as an example, we demonstrate the optimization of the antenna system and its distribution on the wall. Comprehensive multiphysics analyses of the antenna-embedded wall shed light on the intricate relationship between electromagnetic transmission, thermal insulation, and mechanical load-bearing capacity. Beyond modeling the intricate multiphysical relationship, our research also reveals its broader implications for the Internet-of-Things as a key enabler of smart city evolution where seamless cellular connectivity harmonizes with sustainable architecture. Being a tutorial, this article provides an overview of mathematical formulas governing thermal conductance and solid mechanics in analogy to those of electromagnetism. The overview helps us understand the intricate multiphysical design of innovative antenna-embedded building elements.

Digital Object Identifier 10.1109/MAP.2025.3610073

INTRODUCTION

The use of cellular networks is increasing globally. Speaking of Finland, the average consumer used roughly 32 Gb per month in 2022 [1]. Globally, mobile Internet use is 58.5% of total Internet use [2], where many users rely on cellular networks as their main Internet access. Meanwhile, the European Union has introduced directives on nearly zero-energy building [3] to fight against global warming. The directive aims to limit the energy use of buildings utilizing, e.g., better thermal insulation

requirements. All new buildings need to fulfill zero-emission building requirements by 2030. To achieve new nearly zero-energy building and zero-emission building requirements, energy-efficient buildings are equipped with highly insulated envelopes and well-sealed structures: e.g., thicker insulation layers, low-emissivity air-tight windows, and multilayer heat insulation systems. These envelopes, unfortunately, have tremendous implications on our experience of mobile Internet through cellular networks because they block radio signals and make the outdoor-to-indoor (O2I) communication challenging if not impossible in the future [4], [5]. Simultaneously, surveys, such as in [6] and [7], reveal that a significant number of mobile users face poor connectivity in both residential and workplace environments. It is logical to assume that this issue may be exacerbated with the implementation of higher carrier frequencies due to the reported higher O2I entry loss [4], [5].

To enhance O2I communication, research over the past decade has explored both active and passive solutions. Active solutions, including indoor base stations [8], [9], [10] and repeaters [11], [12], [13], often necessitate a radio frequency-over-fiber network, resulting in high costs and increased energy consumption by the active electrical components. In contrast, passive solutions, exemplified by low-emissivity windows incorporating frequency-selective surfaces [14], [15] or signal slots [16], [17], operate without an additional energy source. However, a common challenge with passive solutions is that they tend to have relatively narrow passbands within the radio frequency spectrum.

Our solution to improve O2I communication is a passive antenna system embedded into an external building wall, called a *signal-transmissive wall*, which we have been studying in recent publications [18], [19], [20], [21], [22], [23]. The idea of signal-transmissive walls is to create a more effective alternative path for electromagnetic waves to propagate into the building. Transmission losses caused by external building walls are known to be significant [24], especially when the thickness of concrete layers is increased, so creating other, lower loss, paths is necessary to make the building more radio-transparent for indoor cellular users. In the signal-transmissive wall, an antenna element captures a portion of the incoming electromagnetic wave and transmits the power via coaxial cable, for example to a second antenna on the other side of the wall that reradiates the power. The embedded antenna system should improve the transmission by making sure that the antenna elements capture as much incident power and that the coaxial cable has a significantly lower loss than the raw building wall.

Antennas cannot just be embedded in a building wall without considering their effects on other essential properties of the wall. The wall must be able to, e.g., keep indoor temperature, insulate street noise and moisture out, and support the weight of itself or even the whole building structure. Embedded antenna systems should not influence these properties of the raw wall. Analyzing a building wall is a multiphysical problem that this tutorial gives insights into. The novelty of this tutorial is the solid mechanics study of the wall in addition to the electromagnetic and thermal studies [18], [19], [20], [21], [22], [23]. As a multiphysics study is an intricate problem, this tutorial summarizes mathematical quantities and governing rules of each physics domain for proper understanding of the problem at hand. Table 1 lists the physics domains of our analysis, their important quantities, and governing rules. Analogous to electromagnetics, the field, its gradient, and flux are also important when studying solid mechanics and heat transfer. The three domains are interlocked to each other, having us to find a compromise of the performance of the signal-transmissive wall. We show novel and robust designs of an antenna system, comprising an antenna element, array, and decoupling cavity for the purpose, thereby an important tradeoff between electromagnetic and thermal performance of the signal-transmissive wall is revealed, and also simultaneous optimization of the electromagnetics and solid mechanics performance of the same is realized. Multiphysical analysis of building infrastructure with embedded antenna systems is an unexplored field, according to the survey article [25], that this article addresses.

To study the signal-transmissive wall, we have decided to use a load-bearing concrete sandwich wall in our examples, as illustrated in Figure 1. The load-bearing wall is usually installed as an outer wall of buildings, composed of 220-mm-thick mineral wool sandwiched between 70-mm and 150-mm concrete slabs, where the thicker concrete slab is the load-bearing element. This load-bearing wall element is widely used in Finland.

The remainder of this article consists of three sections. The "Theory" section delves into the essential electromagnetic, heat transfer, and solid mechanics theories pertinent to building walls and antenna-embedded walls. This section establishes the theoretical foundation for understanding the multiphysical characteristics of these structures. Following the theoretical framework, the "Practical Examples of the Signal-Transmissive

TABLE 1. DIFFERENT PHYSICS, QUANTITIES, AND RULES. SOLID MECHANICS AND HEAT TRANSFER IN CASE OF STATIONARITY.

Physics	Field	Gradient	Flux	Rule
Solid mechanics	Displacement (vector) ($\vec{u}$)	Strain (tensor) ($\boldsymbol{\varepsilon}$)	Stress (tensor) ($\boldsymbol{\sigma}$)	Cauchy's stress theorem
Heat transfer	Temperature (scalar) (T)	Temperature gradient (vector) ($\overrightarrow{\nabla T}$)	Heat flux (vector) ($\vec{q}$)	Fourier's law of thermal conduction
Electromagnetics	Electric potential (scalar) (V)	Electric field (vector) ($\vec{E}$)	Electric displacement (vector) ($\vec{D}$)	Maxwell's equations

Wall" section provides practical insights, exploring various material choices for coaxial cables and their impact on both thermal transmittance and electromagnetic transmission coefficients. Moreover, the mechanical load distribution of antenna-embedded walls is scrutinized in comparison to bare load-bearing walls, assessing the stress concentration factor (SCF) as a key metric. The tutorial concludes in the final section, summarizing the key findings and insights derived from the analyses.

As notations, while a scalar quantity is represented by an italic font like s, vector and tensor quantities are denoted with the upper arrows $\vec{s}$ and with bold faced $\mathbf{s}$, respectively.

THEORY

In this section, we cover the essential electromagnetic, thermal, and structural mechanics theory related to building walls. Table 1 gathers all of the physics and quantities related to them as well as the rules behind them, which we address in this work. In the realm of steady-state heat transfer and solid mechanics, the application of a direct current analogy proves pertinent, drawing parallels between phenomena, such as thermal conduction, structural deformation, and the steady flow of current in electrical circuits. Conversely, within the domain of electromagnetic analysis for communication studies, the analytical focus shifts to considerations of alternating current phenomena represented by frequency, phase, and wave propagation, elucidating the behavior of signals within the communication medium.

ELECTROMAGNETIC TRANSMISSION

The normal building wall consists of multiple dielectric slabs next to each other. These layers are characterized by relative permittivity ε_r, electrical conductivity σ_r, and thickness d. Relative permittivity corresponds to electric polarizability, whereas conductivity relates to the losses of a dielectric material. Normal building materials are nonionized and nonmagnetic so material permeability μ can be assumed to be the permeability of free space μ_0. The International Telecommunication Union (ITU) recommendation P.2040 [26] gives an empirical model to calculate dielectric parameters of most common building materials, such as concrete, Rockwool, and glass, over the frequency range

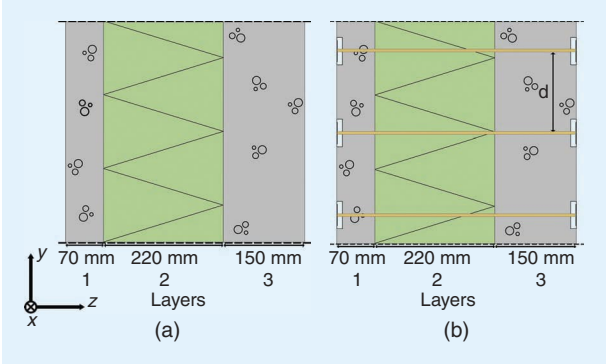

FIGURE 1. (a) Concrete sandwich load-bearing wall and (b) signal-transmissive wall. Layer 1 is outdoor-facing concrete, layer 2 is thermal insulating mineral wool, and layer 3 is the indoor-facing load-bearing concrete layer.

of 100 MHz up to 100 GHz and beyond. This model is obtained by applying a linear regression on a dual-logarithmic graph of all the available measured complex permittivity estimates.

To be able to estimate the transmission coefficient of a building wall, some assumptions need to be made. First, the wall needs to be sufficiently large so that no other radio signal paths, like edge diffraction, affect the transmission coefficient. Second, the source is assumed to be a plane wave to simplify the calculation of the transmission problem like it is performed in the ITU-R P.2040. Third, the material layers are assumed to be homogeneous and isotropic. Last, the surface of the wall is assumed to be smooth and planar, i.e., their roughness is 1/50 of the wavelength of a radio signal as a rule of thumb, so that scattering of an incident plane wave on the surface is negligible. While the assumptions of a smooth surface may hold for lower frequencies, they become increasingly invalid at higher frequencies, such as millimeter-wave (mmWave) bands, as surface roughness may become comparable to the wavelength. However, for the frequencies targeted in this study, these assumptions remain reasonable for evaluating the performance of the antenna system embedded in the wall because the surface roughness has a negligible effect on the antenna system itself, and also because most of the power propagating through the wall is captured by the antennas at these higher frequencies. More power of an incident wave is scattered on a rough surface, leading to less power penetrating into the wall. Therefore, the flat smooth surface model of the wall provides the most modest evaluation of the benefit of the embedded antenna systems for improving the transmission coefficients.

In the building wall modeled as a multilayered dielectric slab, the incoming and transmitting wave undergoes reflection and transmission at every material interface inside the wall, causing a standing wave. The transmission coefficient of the wall can be estimated by analytical methods, like the one in ITU-R P.2040, or by using full-wave simulations using the Floquet theory. The advantage of using the Floquet theory is that it can simulate a transmission loss of a virtually infinitely large wall, similarly to the analytical calculation of the same using ITU-R P.2040. The infinitesimally large wall is a repetition of a unit cell wall around itself in x and y directions, where the z direction is the propagation direction of an electromagnetic wave, according to the coordinate system in Figure 1(a). In popular electromagnetic numerical simulation tools, such as *CST Studio Suite* and *Comsol multiphysics*, such a repetition of a unit cell is set by the unit cell boundary.

When using numerical full-wave simulations with unit cell boundaries, the electromagnetic field at any point in the unit cell is considered as a Fourier series whose basis functions are the Floquet modes [27]. Unlike in waveguides, the group velocities of Floquet modes are constant but the phase velocities vary across the modes. The total field at any point in the unit cell is obtained by summing up the coefficients of all the Floquet modes. In order for the solved total field to satisfy the Maxwell equations and boundary conditions, all of the propagating Floquet modes must be considered. In practice, if unit cell dimensions are smaller than the wavelength for a normal incidence

plane wave, only the fundamental modes can be supported in the unit cell. However, higher-order modes can propagate if the dimensions are greater than the wavelength or for a glazing incident angle of a plane wave.

THERMAL INSULATION

Heat transfer from the hotter to the colder side of the object is called *thermal conduction*. All materials have different capabilities to conduct heat, which is described by thermal conductivity [W/(m·K)], denoted by a symbol λ in ISO 6946 [28]. Thermal conductivity and electrical conductivity correlate approximately with each other in the case of metals according to the Wiedemann-Franz law. This correlation is based on the fact that freely moving valence electrons transfer not only electrical current but also heat. This correlation does not hold for other materials due to the increased importance of phonon carriers for heat in nonmetallic materials [29].

The Fourier's law of heat conduction describes a linear conductive heat flux through a material

$$\vec{q} = -\lambda \cdot \overrightarrow{\Delta T} \tag{1}$$

where $\vec{q}$ presents the heat flux vector. For problems where temperature variation is confined to 1D, such as along the z-coordinate direction, the Fourier's Law of heat conduction can be simplified as

$$\vec{q} = -\lambda \frac{dT}{dX} = -\lambda \frac{(\overrightarrow{\Delta T})}{d}. \tag{2}$$

Heat conduction is approximated as 1D when conduction is significant in one dimension only, which is the case of building walls where the heat transfer path from indoor to outdoor direction is much shorter than the paths along the other two dimensions, owing to the much larger dimensions in those directions, ensuring validity of the analytical calculations and numerical simulations of this article.

Often, material thickness over thermal conductivity, i.e., d/λ, is defined to be thermal resistance and therefore the 1D Fourier's law is a discrete analogy of Ohm's law. Thermal transmittance, which is also called *U-value* [$W/m^2 \cdot K$], is an often-used metric to describe the thermal insulation of building walls. Thermal transmittance is defined to be an inverse of the total thermal resistance of the object [28]. In the example raw load-bearing building wall of this study, material layers are sandwiched together, i.e., piled over, so the thermal resistances are considered a series and hence the total resistance is a sum of them, as shown in Figure 2. Now, recalling that the temperature gradient is inherently a purely real value, as previously discussed, we can treat our equivalent thermal circuit as a direct current circuit: i.e., there are no reflections between layers.

When calculating the thermal transmittance of a building wall, their internal and external surface resistances, R_{si} and R_{se}, respectively, need to be defined. They refer to indoor- and outdoor-facing sides of the wall and represent the surface convective and radiative coefficients. When the direction of heat flow is horizontal, like in the case of a wall, ISO 6946 defines R_{si} to be $0.13\ m^2 \cdot K/W$ and R_{se} to be $0.04\ m^2 \cdot K/W$.

The signal-transmissive wall has electric components going through multiple layers, such as a waveguide or a coaxial cable. Similarly, as in the electromagnetic analysis, the wall can be modeled as repeated unit cells that are copied around itself. The thermal resistance of the signal-transmissive wall is modeled by a series of parallel-connection resistances of the wall and electric components, as illustrated in Figure 2 [21]. This

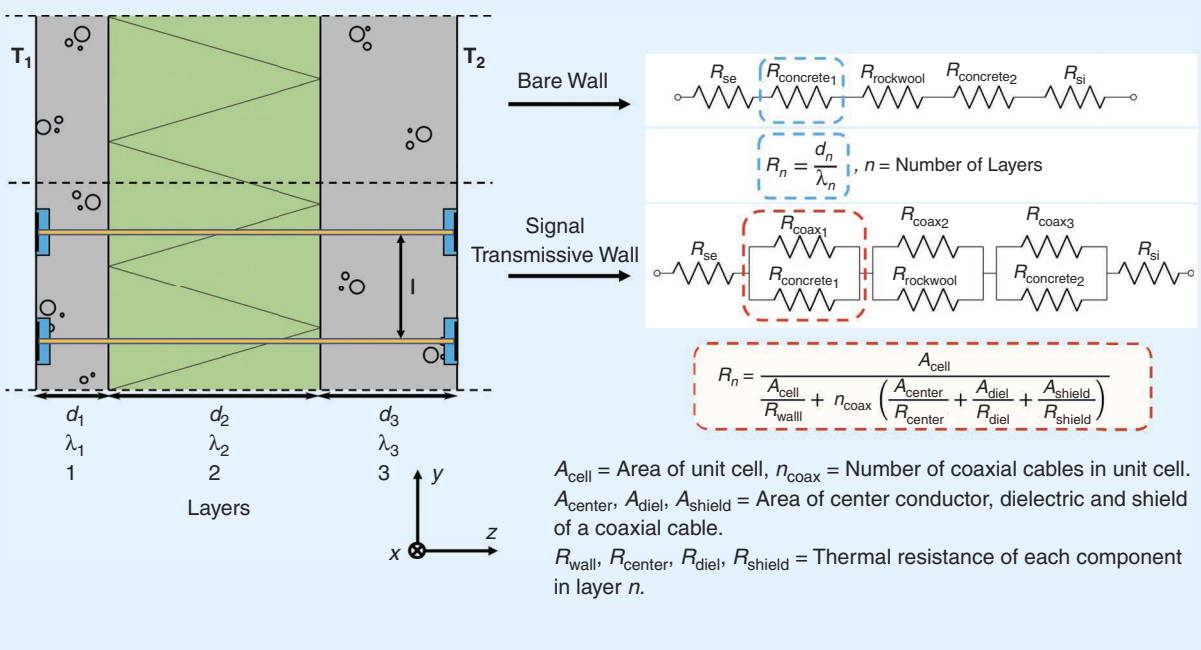

FIGURE 2. Example of three-layer wall structure, signal-transmissive wall, and equivalent thermal circuits.

approach enables heat flux transfer between the wall layers and the coaxial cable at the interfaces, enhancing accuracy compared to other modeling methods, especially when there is a significant difference in thermal conductivities among the materials [22]. The surface areas that the electric components occupy on the *xy*-plane of the wall, according to the coordinate system in Figure 1(a), determines the corresponding resistance. The resistance of the signal-transmissive wall is calculated in the same way as in electrical circuits. It is good to note that thin layers, whose thermal resistance is in series with the wall, such as planar antennas on the *xy*-plane, have a negligible effect on total thermal transmittance. This is because the thermal resistance of these thin layers is negligible, as illustrated in (2). For this reason, the thermal analysis of the signal-transmissive wall focuses only on the embedded coaxial cables that have much larger thermal resistance than the antenna elements.

STRESS DISTRIBUTION IN THE LOAD-BEARING WALL

In this tutorial, we evaluate a mechanical stress distribution of the bearing wall. The mechanical analysis focuses solely on the load-bearing concrete layer located at the inner part of the wall, which carries the majority of the building's load. The outer concrete layer and mineral wool, while important for structural enclosures and insulation, do not contribute as significantly to load bearing and, hence, are excluded from this analysis. By modeling the concrete as an isotropic linear elastic material, we describe its stiffness by introducing the Young's modulus (E) [Pa] and the Poisson's ratio (ν) [a.u].

The Young's modulus measures the tensile or compressive stiffness of a solid material under uniaxial loading. The Poisson's ratio provides a measure of the relative expansion or contraction in the directions perpendicular to a direction of loading. The shear modulus G [Pa] relates Young's modulus and Poisson's ratio as $G = E/\{2(1+\nu)\}$ and provide the relationship between shear stress and strain.

Through these elastic parameters, it is possible to define a linear relationship, e.g., the constitutive relationship, to link the stress and the strain within the material at a point level. Such a relationship can well approximate the true nonlinear stress–strain behavior of concrete under compressive and tensile stress, provided that stresses do not reach values close to the material strength. Note that stress and strain have a tensorial nature, e.g., the stress tensor defined in a Cartesian coordinate system at any place on/in the specimen is

$$\boldsymbol{\sigma} = \begin{bmatrix} \sigma_{xx} & \tau_{xy} & \tau_{xz} \\ \tau_{yx} & \sigma_{yy} & \tau_{yz} \\ \tau_{zx} & \tau_{zy} & \sigma_{zz} \end{bmatrix} \tag{3}$$

where the double subscript in each stress component is used to denote the directions of the stress and the normal to the plane where the stress is acting, respectively. For example, σ_{xx} describes the stress component in the x direction on a plane with normal vector $\hat{x}$, namely a normal stress, while τ_{xy} describes the stress component in the y direction on a plane with normal vector $\hat{x}$, namely a shear stress. The stress components in a point depend on the orientation of the coordinate system. Notably, for every point in a stressed specimen there exist at least three planes, called *principal planes*. These planes are associated with normal vectors, the so-called principal directions (1, 2, 3), where the corresponding stress vector has the same direction as the normal vector, namely planes where the shear stresses are null. The three principal directions are not always orthogonal to each other, unlike the Cartesian coordinate system. The three stresses normal to the principal planes are called *principal stresses* (σ_{11}, σ_{22}, σ_{33}). The concept of principal stresses is often used [30] to analyze the stress state of a specimen.

For brittle materials like concrete, little inelastic deformations are observed before failure, namely before the stress reaches the material strength. Indeed, concrete has a poor tensile strength, much lower, i.e., about 1/10, than the one in compression [30]. This fact motivates the use of reinforcing steel metal bars and nets in concrete elements. Nonetheless, in the following preliminary analysis, when comparing walls with and without antenna systems, we neglect the reinforcement metal bars and net for both walls with and without antenna systems.

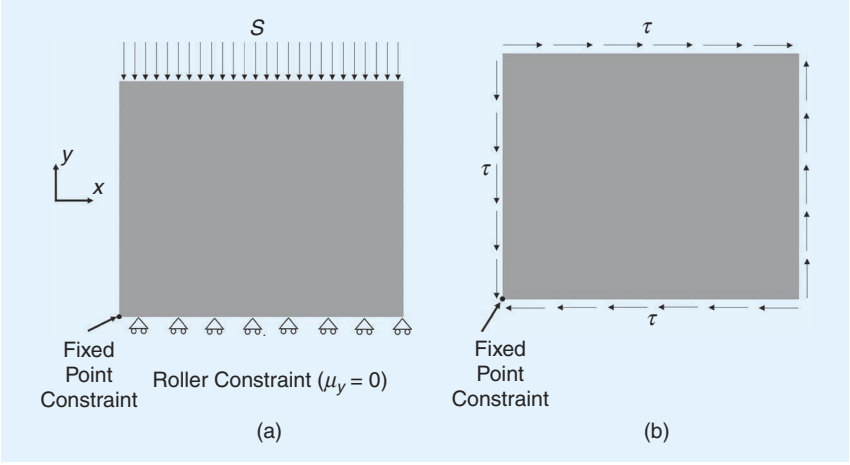

FIGURE 3. (a) Vertical loading scenario and (b) pure shear stress scenario. S is the applied stress and τ is shear stress. The gray block is a slab of concrete.

Two different 2D loading scenarios are commonly adopted to assess the performance of a wall: The first one looks at the gravity loads, whereas the second one to the actions generated by horizontal displacements imposed at the wall base. In testing and simulations, these two scenarios are realized by creating a uniaxial and a pure shear state loading.

In the performed analyses the first scenario, illustrated in Figure 3(a), considers a uniform load distribution (S) applied on the top side of the wall and acting along the vertical (y) direction. In this case, the other side of the wall is

constrained to impede displacement along the vertical direction by using rollers ($\mu_y = 0$). The second case is achieved by applying uniform load distributions acting along a direction tangential to the wall surface, mimicking a situation where the object is pulled from one corner and is fixed from the opposite corner [Figure 3(b)].

In the case of a vertical loading scenario, the only nonnull stress component is σ_{yy}, which leads to a principal directional along the vertical direction, namely a principal stress component along the y direction. Conversely, for pure shear loading, the principal directions are rotated of 45° with respect to the x-y Cartesian axis and the related principal stresses are $\pm\tau$. For instance, the stress ($\sigma_{yy} = \sigma_{11}$) distribution due to a vertical loading $S = 1$ [Pa] is shown in the bottom part of Figure 4.

If an object, the wall in this case, has mechanical/geometrical irregularities or discontinuities stress concentration "around" them is observed. The SCF, K_t [a.u.], is a metric used to denote the difference between peak and nominal stresses related to the object with and without discontinuities, respectively [31]. For example, the stress concentration due to a circular hole in an infinitely large plate under uniaxial loading is equal to

$$K_t = \frac{\sigma_{\text{peak}}}{\sigma_{\text{nominal}}} = 3 \tag{4}$$

where σ_{peak} is the peak stress on the edge of the hole along the load direction, whereas σ_{nominal} is nominal stress on the structure under the same load without a circular hole [31]. In our study, multiple small circular holes and cavities are introduced in the concrete slab to accommodate the coaxial cables and cavities behind the antenna elements. We compute the SCF over the whole wall domain by performing linear static simulations of the loaded wall with and without holes or cavities. The SCF is obtained by dividing the stress fields of the two cases, namely with and without holes or cavities. For instance, for the case discussed in Figure 3(a), the distributions of σ_{11} for the cases with and without the holes for coaxial cable, as well as the K_t, are shown in Figure 4.

PRACTICAL EXAMPLES OF THE SIGNAL-TRANSMISSIVE WALL

Next, we give practical examples of antenna-embedded wall using our design called a *signal-transmissive wall*. The signal-transmissive wall, where passive antenna elements were embedded back-to-back to a load-bearing concrete sandwich wall, has been discussed in terms of electromagnetic transmission and thermal insulation in our previous articles [18], [19], [20], [21], [22], [23]. They are evaluated using analytical models presented in [21] and [23], and mechanical examples are simulated using *Comsol multiphysics*.

ELECTROMAGNETIC TRANSMISSION AND THERMAL INSULATION OF SIGNAL-TRANSMISSIVE WALL

An antenna element is an important part of a signal-transmissive wall. The question "What is a good antenna element?" is important. Most antenna elements are resonant-based with relatively large ground planes, hence limiting the bandwidth. Resonant-based antennas are not ideal for the antenna-embedded wall since cellular radios use a wide range of frequencies that the narrow bandwidth of resonant antennas cannot support. Moreover, the large ground plane acts as a reflector for frequencies

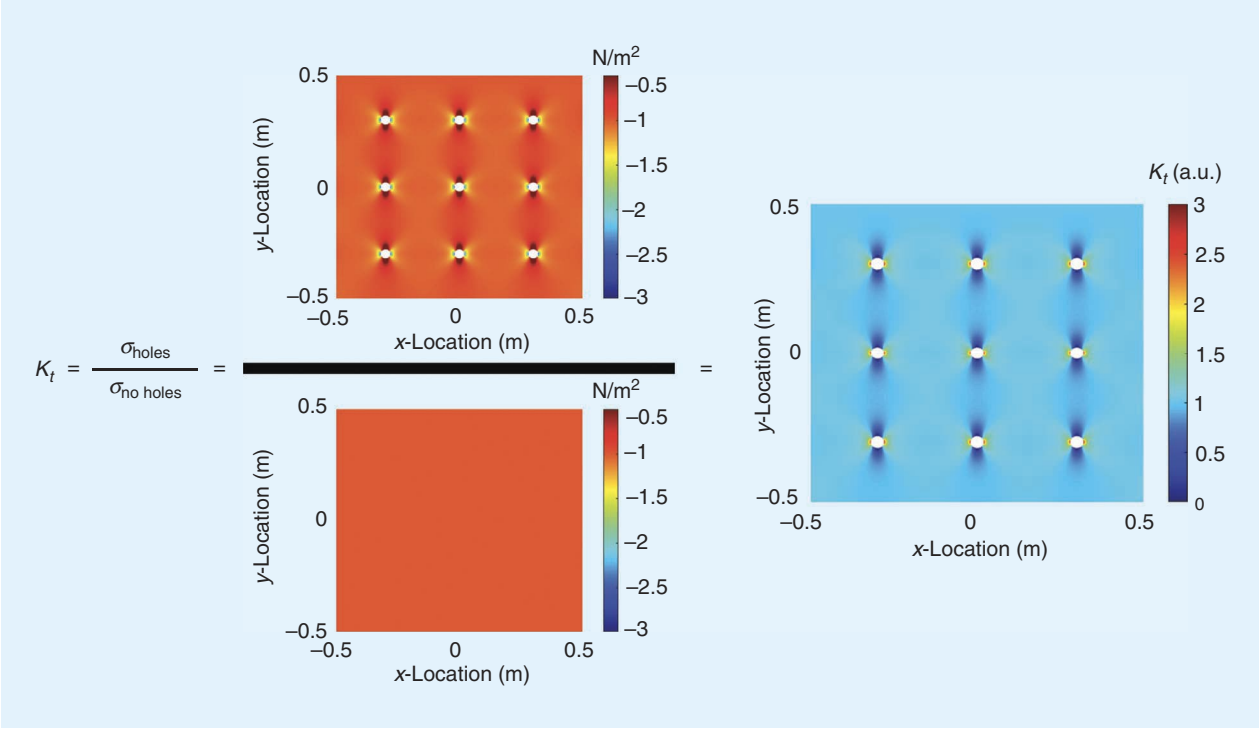

FIGURE 4. Calculation of SCF K_t [a.u.] using numerical simulations for the loading case shown in Figure 3(a).

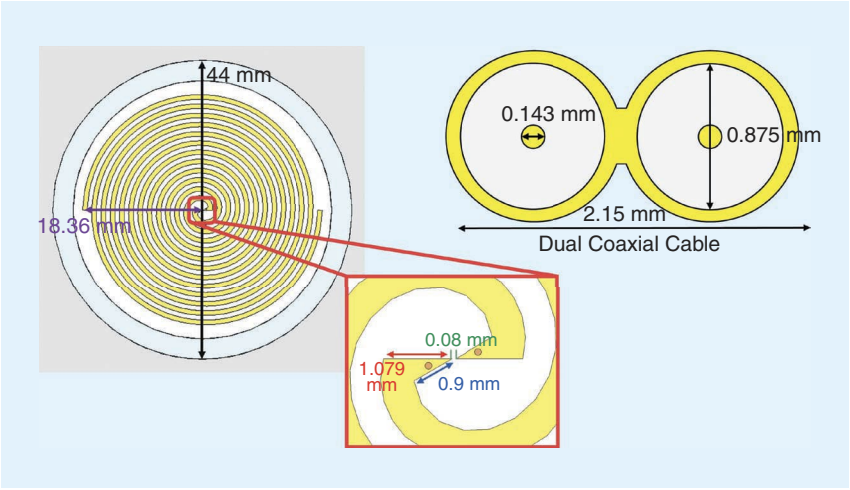

FIGURE 5. The Archimedean spiral antenna element and dual-coaxial cable. White color represents PCB, yellow is copper, and gray is concrete.

other than the resonant frequency, increasing the reflectivity of the building wall, and thus less power can penetrate the building. As the lifespan of a building is more than 100 years and buildings are renovated roughly every 40 years, antenna systems embedded in the building wall should operate at least until the next renovation and be forward-compatible so that they can support possible future cellular frequency bands in addition to legacy bands. Several nonresonant-based antennas, like self-complementary antennas and spiral antennas, show constant input impedance over the ultrawide bandwidth. Self-complimentary antennas do not have a ground plane, so they do not block incident fields but they tend to radiate two equal lobes toward both broadside directions to the plane of the antenna element. This leads to high coupling with the building wall, and often low efficiency, when placed on a building wall. To mitigate these effects, various strategies can be employed to decouple the antenna element from the wall, such as incorporating a foam cavity behind the antenna element, which helps to enhance radiation efficiency [19].

An Archimedean spiral antenna is an interesting candidate as an element of antenna-embedded walls. Spiral antennas are naturally circularly polarized, allowing them to receive two linear polarizations too. Also, spiral antennas are in general smaller than linearly polarized self-complementary antennas, like bow-tie or log periodic tooth antennas, especially if considering dual-polarized elements. An Archimedean spiral antenna needs roughly a four times smaller footprint than a dual-polarized bow-tie antenna. The size of the antenna element is important when considering the mutual coupling between antenna elements. Smaller antennas can be implemented on a wall surface more densely than large antennas. Coupling between antenna elements needs to be derived in the numerical full-wave simulations using the unit cell boundary.

In our work, we therefore concentrate on an Archimedean spiral antenna element that would operate from ~2.6 GHz up to mmWaves, shown in Figure 5 [23]. Our Archimedean spiral has six rounds with right-handed circular polarization. The outer radius of the designed spiral antenna is 18.36 mm and the inner radius of 1.079 mm with triangular tuning elements, ensuring stable input impedance over the frequency range. The antenna is realized on top of circular Rogers RT-duroid 5880 laminate, whose relative permittivity is 2.2 and loss tangent is 0.0009, with a diameter of 38 mm. The antenna element is backed with a half elliptic foam cavity whose depth is 8.5 mm.

Usually balanced antennas, like spiral antennas, are used with a balun to connect to unbalanced coaxial cables. In a back-to-back antenna system, we can connect between antenna elements using a balanced dual coaxial cable and avoid balun. The balanced cable consists of two coaxial cables where their shields are soldered to each other and, hence, its characteristic impedance is twice the impedance of a single cable. Since the spiral antenna has an input impedance of ~160 Ω when placed on top of a concrete slab, soldering the shields of two coaxial cables whose characteristic impedance is close to 80 Ω should ensure good matching between antenna elements and the dual coaxial cable. The center conductors of both coaxial cables are soldered to each leg of the spiral antenna. To fit the dual coaxial cable to the feed gap of the spiral antenna, we used two coaxial cables with 1.075-mm diameter and low-density PTFE (Polytetrafluoroethylene), whose relative permittivity is 1.75 and loss tangent is 0.0002 and a characteristic impedance close to 82 Ω. Figure 6 shows the attenuation of the coaxial cable consisting of different materials. The material types have a huge effect on the attenuation. The lower conductivity of the shield does not affect the attenuation as much as the center conductor material, since the currents mostly flow on the center conductor.

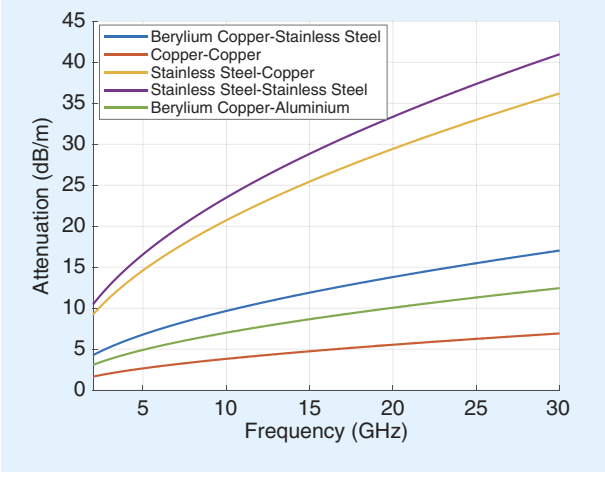

FIGURE 6. Attenuation of a coaxial cable whose diameter is 1.075 mm. The label has first the material of the center conductor and then the shield.

When coaxial cables are integrated into a wall, their material types also affect the U-value of the wall. The U-value of the signal-transmissive wall was calculated for different material combinations of the shielding and center conductors of the coaxial cables. We determined the maximum allowable density of back-to-back antenna systems by adjusting the spacing between antennas. This adjustment ensures that the U-value of the wall remains below the 0.17 $W/m^2 \cdot K$ limit specified by Finnish building regulations [32], considering the conductor materials used in the coaxial cables. By carefully managing the separation between antennas, we can maximize the number of antennas in the wall while staying within the thermal limits. Table 2 shows the maximum number of cables that can be embedded in 1 m^2 area. As can be seen, the maximum number of cables depends a lot on the material combinations in the cables. Since the volume of the shield is 19 times larger than the center conductor, it is important to use low thermal conductivity material for the shield.

Figure 7 shows the transmission coefficient of the antenna-embedded wall with different coaxial cable assemblies. The best assembly is a tradeoff between large electromagnetic transmission coefficients and low thermal transmission, represented by U-values. Although the number of embedded stainless-steel cables is the largest according to Table 2, the largest transmission coefficient is achieved with the beryllium copper–stainless steel cable assembly. On average beryllium copper–stainless steel assembly gives 8.6-dB and 10.6-dB larger transmission coefficient than the stainless steel and normal copper cables, respectively.

MECHANICAL LOAD DISTRIBUTION OF SIGNAL-TRANSMISSIVE WALL

SIMULATION SETUP

The stress distribution of the load-bearing wall and the signal-transmissive wall is studied through numerical simulations using Comsol multiphysics. We focus on the impacts of 1) the dual-coaxial cables and 2) cavity shape on the load-bearing 150-mm-thick concrete. The solid mechanics simulation does not allow infinitely large wall but only of a finite size. In the case of coaxial cables, a 2D linear static simulation with the mentioned thickness was performed. The simulation solves the Cauchy momentum equation at each mesh cell to derive the displacement vector. The simulation model is a 1 × 1 m^2 slab of concrete whose Young's modulus is 25 GPa and Poison ratio of 0.2. Dual-coaxial cables are embedded every 15 cm so that one of the cables is at the center of the concrete slab and no cables are embedded closer than 15 cm from the edges. This will lead to 25 cables in the concrete slab. The shield of the coaxial cables is stainless steel whose Young's modulus is 200 GPa and Poison ratio of 0.29. Since stainless steel is much harder than PTFE as the insulating dielectric material of the coaxial cable, the cables can be modeled as hollow stainless-steel tubes.

The second simulation setup analyzes the impact of cavity shape on the SCF using 3D simulations. The antenna element is installed inside a foam-filled cavity, which mechanically isolates it from the surrounding concrete and ensures that local stress does not directly affect the performance of antenna element. For this reason, the antenna itself is not included in the mechanical simulations. In our previous study [23], we showed that changing the cavity shape from rectangular to ellipsoidal does not affect the antenna's electromagnetic performance. In this study, we focus on comparing the effect of the cavity shape on the SCF. The SCF of the concrete slab was calculated from simulations with and without embedded coaxial cables or cavities. The stress field from simulations of the raw concrete slab without holes is taken as nominal stress and that with coaxial cables as peak stress. The applied boundary load was 1 N/m^2, which induces a constant, nominal, stress of –1 N/m^2 to the raw concrete slab without holes or cavities. The minus sign of the stress value means it is compressive.

RESULTS

First, let us concentrate on 2D simulation with coaxial cable and the vertical loading scenario. Figure 8(a) shows the SCF of the

TABLE 2. THE DENSEST POSSIBLE COAXIAL CABLE INSTALLATION THAT MEET THE SMALLER U-VALUE THAN THE REQUIRED 0.17 $W/M^2 \cdot K$ WITH VARYING METAL TYPES OF THE CENTER CONDUCTOR AND SHIELD ON A LOAD-BEARING WALL.

Center Conductor	Shield	Density [1/m^2]
Beryllium copper	Stainless steel	82.65
Stainless steel	Stainless steel	100
Copper	Copper	4.34
Stainless steel	Copper	4.73
Beryllium copper	Aluminum	7.72

All the cables have low-density PTFE as a dielectric.

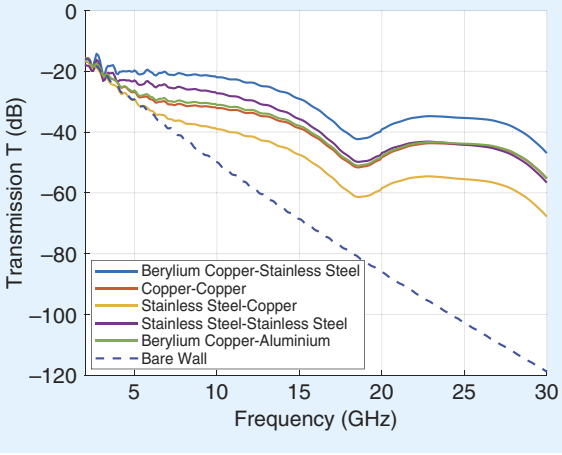

FIGURE 7. Transmission coefficient of a signal-transmissive wall with different coaxial cable materials. The label has first the material of the center conductor and then the shield. Antenna system density is given in Table 2.

signal-transmissive wall near one of the dual-coaxial cables. The maximum SCF of the concrete part is 1.8 roughly at the top-right and top-left sides of the dual coaxial cable. Similarly, the maximum SCF of the coaxial cable part is 9.3 located at the left- and rightmost parts of the dual coaxial cable. It is necessary to design a concrete slab so that it endures 80% higher peak stress than that observed with ordinal plane uniform slab for the vertical load conditions. It is good to notice that stress drops to the nominal level within 1 mm away from the coaxial cable, meaning that the nominal stress is not increased by the coaxial cables. The increased stress can be managed by choosing the right concrete material as is practiced in manufacturing concrete walls with cavities and holes for ordinal buildings.

Next, Figure 8(b) shows the SCF of the signal-transmissive wall near one cable under the pure shear stress. The maximum SCF of concrete under pure shear stress is 2.3 and it can be found on the top, bottom, left, and right sides of the dual-coaxial cable. SCF in the concrete returns to nominal stress 1 mm away from the cable. The maximum SCF in the coaxial cable is 16 located on the top-right and bottom-left sides at the inner surface of the dual-coaxial cable. The high stress in the stainless-steel coaxial cable is caused by its much higher stiffness compared to the surrounding concrete. This stress is localized within the steel and remains well within its elastic limit, and therefore does not compromise the structural integrity of the wall. In the same way as the vertical loading scenario, the increased peak SCF in the concrete can be easily managed by choosing more enduring concrete slab as exercised in the construction industry.

The maximum SCF on the coaxial cable is 16 located at the top-right and bottom-left sides at the inner surface of the dual-coaxial cable. The high stress in the stainless-steel coaxial cable is caused by its much higher stiffness compared to the surrounding concrete. This stress is localized within the steel and remains well within its elastic limit, and therefore does not compromise the structural integrity of the wall. In the same way as the vertical loading scenario, the increased peak SCF can be easily managed by choosing more enduring concrete slab as exercised in the construction industry.

Figure 9 shows the SCF near rectangular and elliptic cavities. The cut planes are positioned to intersect at the center of cavity. The contours show a 5% increase in SCF relative to the nominal stress. In the case of the rectangular cavity, the maximum SCF is 5.5, located at the corners of the cavity. This meets our intuition, as sharp corners cause a large discontinuity in stress flow. For the elliptic cavity, the maximum SCF is 1.5, located at the left- and rightmost parts of the cavity. This SCF is much lower than that observed for the rectangular cavity, as anticipated.

Finally, Figure 10 shows the SCF near both cavity shapes under pure shear stress. For the elliptic cavity, the maximum SCF is 1.8, which is similar to the vertical loading scenario. While much higher maximum SCF of 20.8 is observed in the top-left and bottom-right corners for the rectangular cavity. This high SCF could lead to cracking, unless additional strengthening, such as metal meshing of the concrete, is implemented. Overall, we conclude that changing the cavity shape from rectangle to ellipsoid significantly lowers the SCF, improving the wall's structural integrity while keeping electrical and thermal performance of the signal-transmissive wall. The increased stress concentration caused by the coaxial cables and elliptic cavity can effectively be managed by ordinal concrete material.

CONCLUSIONS

In this tutorial, we have introduced the antenna-embedded wall and its multiphysical analyses so that it could be part of future buildings and cellular networks. The analysis of the building wall covers electromagnetics, heat transfer, and solid mechanics. We find out that electromagnetics and heat transfer characteristics of the wall are interwoven because of the use of metal that improves the transmission coefficients while conducting heat. Through intelligent material choices, we can maximize the electromagnetic transmission through the wall while ensuring the thermal transmittance is below the required by national regulations. Using higher electrical and thermal conductivity material as a center conductor and low-conductivity material as a shield of the coaxial cables was found the best material combination. We introduced methods to analyze the antenna-embedded wall in terms of stress distribution by using the SCF as the metric. Numerical 2D and 3D simulations show only a slight increase in stress in the wall. By choosing an elliptical cavity instead of a

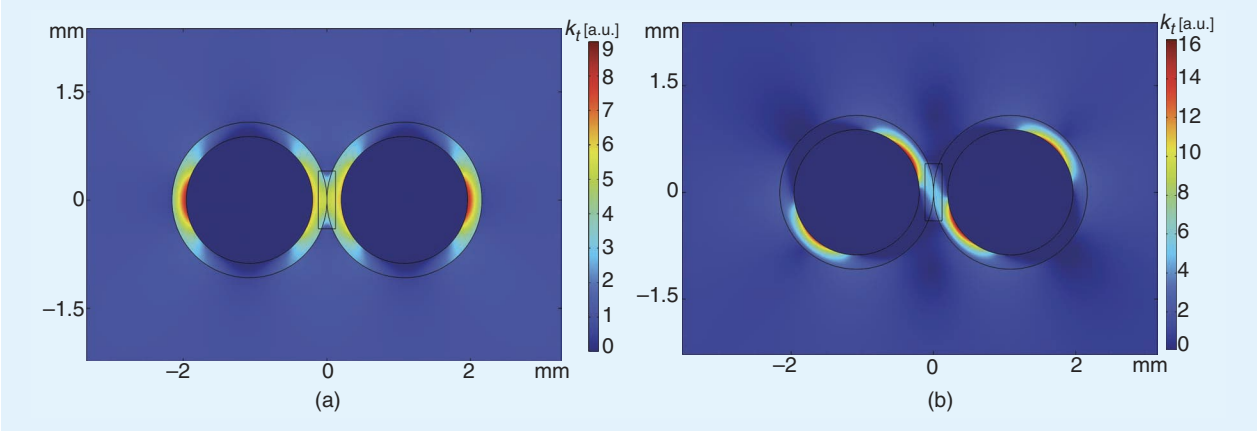

FIGURE 8. SCF: K_t [a.u.], (a) vertical loading and (b) pure shear loading scenario.

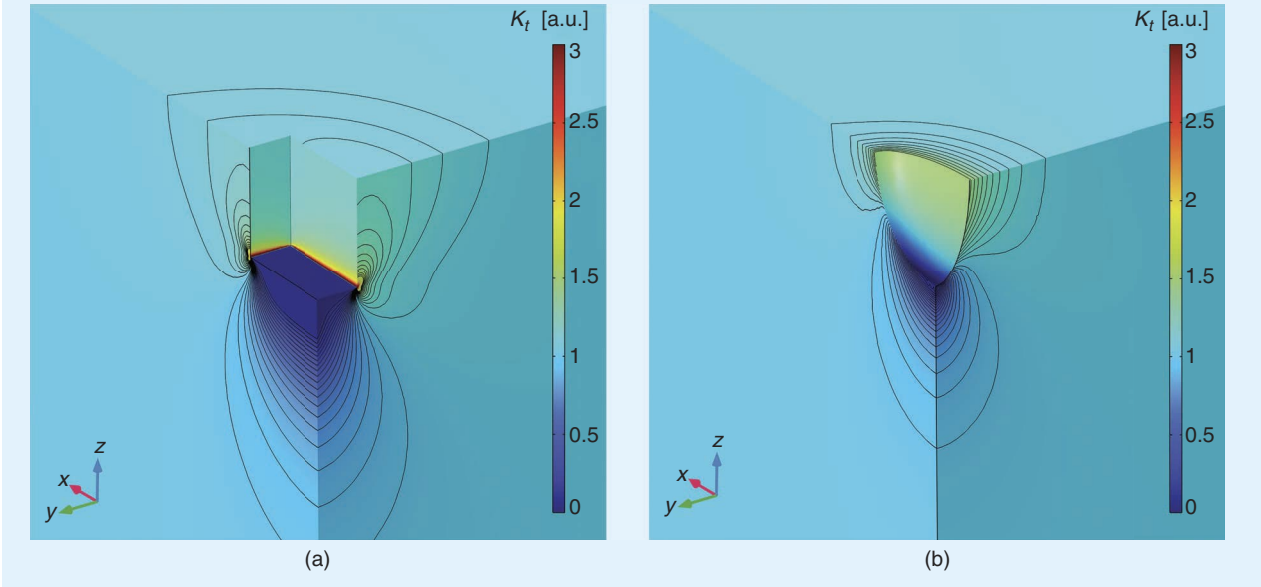

FIGURE 9. SCF: K_t [a.u.], with (a) rectangular and (b) elliptic cavities under vertical loading scenario.

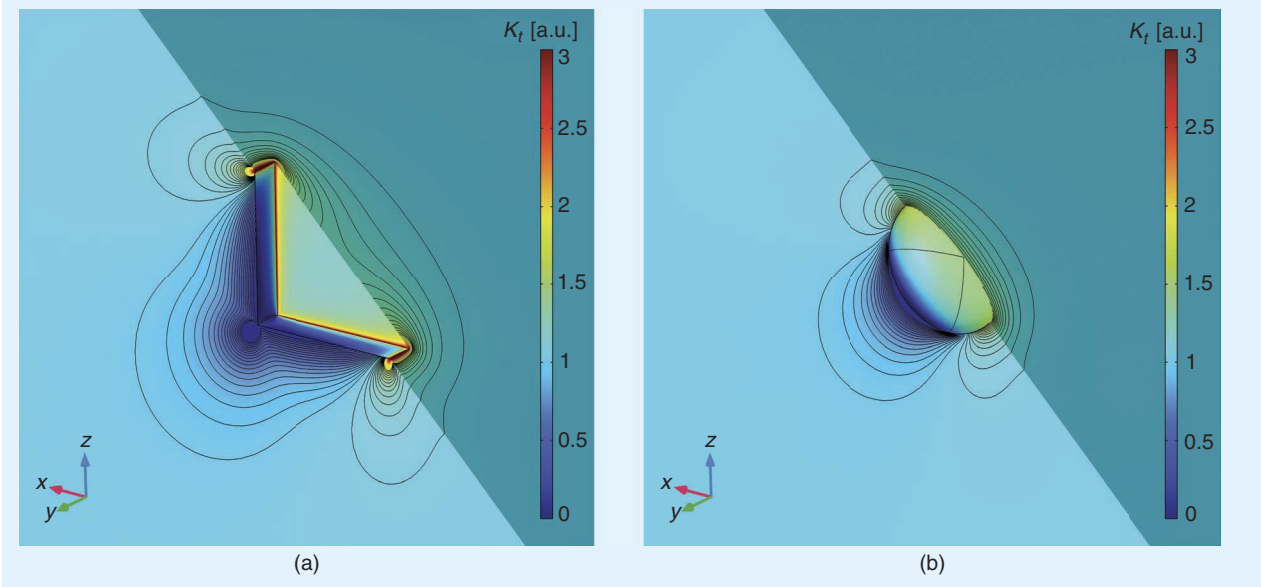

FIGURE 10. SCF: K_t [a.u.], with (a) rectangular and (b) elliptic cavities under pure shear loading scenario.

rectangular one, SCF is significantly reduced, thereby lowering the risk of cracking.

Further multiphysical analyses of the signal-transmissive wall include other relevant physical phenomena, such as acoustics and moisture resistance, which are critical for ensuring the overall performance and durability of antenna-embedded building elements in real-world applications. The signal-transmissive wall is shown to have great potential as part of future cellular networks and smart cities.

ACKNOWLEDGMENT

The work has been supported by the Academy of Finland Research Project "Signal-Transmissive-Walls with Embedded Passive Antennas for Radio-Connected Low-Energy Urban Buildings (STARCLUB)," Decision #323896.

AUTHOR INFORMATION

Lauri Vähä-Savo (lauri.vaha-savo@aalto.fi) is with the Department of Electronics and Nanoengineering, Aalto University-School of Electrical Engineering, 000765 Espoo, Finland. Research interests include outdoor-to-indoor communication, large antenna arrays and multiple input/multiple output for future wireless networks. The author is a Member of IEEE.

Clemens Icheln (clemens.icheln@aalto.fi) is with the Department of Electronics and Nanoengineering, Aalto University-School of Electrical Engineering, 000765 Espoo, Finland.

Research interests include the design and characterization of multielement antennas for wireless communications, from 400 MHz up to millimeter-wave frequencies.

Xiaoshu Lü (xiaoshu.lu@aalto.fi) is with the School of Technology and Innovations, University of Vaasa, FIN-65101 Vaasa, Finland. Research interests include low-carbon strategies and artificial intelligence applications for buildings and districts, focusing on hybrid renewables, energy storage, and waste heat utilization.

Antonio Palermo (antonio.palermo6@unibo.it) is with the Department of Civil, Chemical, Environmental, and Materials Engineering, University of Bologna, 40136 Bologna, Italy. Research interests include solid mechanics and metamaterials for elastic wave control, integrating physics and engineering to design innovative materials and structures.

Alessandro Marzani (alessandro.marzani@unibo.it) is with the Department of Civil, Chemical, Environmental, and Materials Engineering, University of Bologna, 40136 Bologna, Italy. Research interests include structural health monitoring, wave mechanics, and metamaterials, integrating methodologies and technologies for resilient structures and infrastructures.

Katsuyuki Haneda (katsuyuki.haneda@aalto.fi) is with the Department of Electronics and Nanoengineering, Aalto University-School of Electrical Engineering, 000765 Espoo, Finland. The author is a Member of IEEE.

REFERENCES

[1] "Industry analysis #3 2022," Tefficient, Höllviken, Sweden, Jan. 2023. Accessed: Aug. 28, 2025. [Online]. Available: https://tefficient.com/wp-content/uploads/2023/01/Tefficient-industry-analysis-3-2022-mobile-data-usage-and-revenue-1H-2022-per-country-9-January-2023b.pdf

[2] "Mobile internet usage worldwide - Statistics & facts," Statista, Hamburg, Germany, Sep. 2023. Accessed: Aug. 28, 2025. [Online]. Available: https://www.statista.com/topics/779/mobile-internet/#topicOverview

[3] "European Union directive on nearly-zero energy and zero-emission buildings," Eur. Commission, Brussels, Belgium, 2018. [Online]. Available: https://energy.ec.europa.eu/topics/energy-efficiency/energy-performance-buildings/nearly-zero-energy-and-zero-emission-buildings_en

[4] I. Rodriguez, H. C. Nguyen, N. T. K. Jorgensen, T. B. Sorensen, and P. Mogensen, "Radio propagation into modern buildings: Attenuation measurements in the range from 800 MHz to 18 GHz," in *Proc. 80th Veh. Technol. Conf. (VTC-Fall)*, 2014, pp. 1–5, doi: 10.1109/VTCFall.2014.6966147.

[5] K. Haneda et al., "5G 3GPP-like channel models for outdoor urban microcellular and macrocellular environments," in *Proc. IEEE 83rd Veh. Technol. Conf. (VTC Spring)*, 2016, pp. 1–7, doi: 10.1109/VTCSpring.2016.7503971.

[6] "Cellular in the workplace survey, 2017 connectivity issues are widespread," Zinwave, Cambridge, U.K., 2017. [Online]. Available: https://www.ashb.com/wp-content/uploads/2020/04/IS-2017-182.pdf

[7] "Mobile consumer experience," Commission for Commun. Regulation, Dublin, Republic of Ireland, 2022. [Online]. Available: https://www.comreg.ie/media/2022/10/ComReg2283.pdf

[8] S. F. Yunas, "Capacity, energy-efficiency and cost-efficiency aspects of future mobile network deployment solutions," Ph.D. dissertation, Tampere Univ. of Technology, Tampere, Finland, Oct. 2015.

[9] Z. Er-Reguig and H. Ammor, "Towards designing a microcell base station using a software-defined radio platform," in *Proc. 7th Mediterranean Congr. Telecommun. (CMT)*, 2019, pp. 1–4, doi: 10.1109/CMT.2019.8931401.

[10] A. Giovannini et al., "Phase shift impact on the performance of time modulated antenna arrays driven by radio over fiber," *J. Lightw. Technol.*, vol. 39, no. 24, pp. 7761–7770, Dec. 2021, doi: 10.1109/JLT.2021.3098232.

[11] K. Haneda, E. Kahra, S. Wyne, C. Icheln, and P. Vainikainen, "Measurement of loop-back interference channels for outdoor-to-indoor full-duplex radio relays," in *Proc. 4th Eur. Conf. Antennas Propag. (EuCAP)*, Barcelona, Spain, 2010, pp. 1–5.

[12] J. M. Rigelsford, K. L. Ford, and L. Subrt, "A passive system for increasing cellular coverage within energy efficient buildings," in *Proc. 8th Eur. Conf. Antennas Propag. (EuCAP)*, 2014, pp. 614–615, doi: 10.1109/EuCAP.2014.6901833.

[13] K. Ntontin and C. Verikoukis, "Relay-aided outdoor-to-indoor communication in millimeter-wave cellular networks," *IEEE Syst. J.*, vol. 14, no. 2, pp. 2473–2484, Jun. 2020, doi: 10.1109/JSYST.2019.2939745.

[14] A. Asp, A. Baniya, S. F. Yunas, J. Niemelae, and M. Valkama, "Applicability of frequency selective surfaces to enhance mobile network coverage in future energy-efficient built environments," in *Proc. 21th Eur. Wireless Conf.*, 2015, pp. 1–8.

[15] J. Tsuboi et al., "Evaluation of indoor area improvement in the high frequency band using metasurface lenses, FSS technology and relay stations," in *Proc. 95th Veh. Technol. Conf. (VTC-Spring)*, 2022, pp. 1–5, doi: 10.1109/VTC2022-Spring54318.2022.9860922.

[16] "Signal window." Lammin Windows & Doors. Accessed: Aug. 28, 2025. [Online]. Available: http://signal-window.com/

[17] J. Lilja, "Mobile-friendly glass –comparing solutions from the end user viewpoint," in *Proc. Glass Perform. Days (GPD)*, Tampere, Finland, 2019, pp. 1–7.

[18] L. Vähä-Savo et al., "Passive antenna systems embedded into a load bearing wall for improved radio transparency," in *Proc. 50th Eur. Microw. Conf. (EuMC)*, 2021, pp. 424–427, doi: 10.23919/EuMC48046.2021.9338219.

[19] L. Vähä-Savo, K. Haneda, C. Icheln, and X. Lü, "Electromagnetic–thermal analyses of distributed antennas embedded into a load-bearing wall," *IEEE Trans. Antennas Propag.*, vol. 71, no. 8, pp. 6849–6858, Aug. 2023, doi: 10.1109/TAP.2023.3284368.

[20] X. Wang, X. Lü, L. Vähä-Savo, and K. Haneda, "A novel AI-based thermal conductivity predictor in the insulation performance analysis of signal-transmissive wall," *Energies*, vol. 16, no. 10, 2023, Art. no. 4211, doi: 10.3390/en16104211.

[21] L. Veggi, L. Vähä-Savo, K. Haneda, E. M. Vitucci, and V. Degli-Esposti, "Electromagnetic and thermal analysis of coaxial cable connection embedded in an intelligent wall," in *Proc. 17th Eur. Conf. Antennas Propag. (EuCAP)*, Florence, Italy, 2023, pp. 1–5, doi: 10.23919/EuCAP57121.2023.10133233.

[22] T. Lu, L. Vähä-Savo, X. Lü, and K. Haneda, "Thermal impact of 5G antenna systems in sandwich walls," *Energies*, vol. 16, no. 6, Art. no. 2657, 2023, doi: 10.3390/en16062657.

[23] L. Vähä-Savo, L. Veggi, E. M. Vitucci, C. Icheln, V. Degli-Esposti, and K. Haneda, "Analytical characterization of a transmission loss of an antenna-embedded wall," *IEEE Open J. Antennas Propag.*, vol. 5, no. 6, pp. 1765–1772, Dec. 2024, doi: 10.1109/OJAP.2024.3457989.

[24] M. Yang, A. K. Brown, and S. Stavrou, "Resonant behavior of radio-transmission loss due to periodic building structures," *IEEE Trans. Antennas Propag.*, vol. 53, no. 5, pp. 98–105, Oct. 2011, doi: 10.1109/MAP.2011.6138431.

[25] T. Dbouk and O. Mourad, "A review on thermal management and heat dissipation strategies for 5g and 6g base stations: Challenges and solutions," *Energies*, vol. 18, no. 6, 2025, Art. no. 1355, doi: 10.3390/en18061355. [Online]. Available: https://www.mdpi.com/1996-1073/18/6/1355

[26] "Effects of building materials and structures on radiowave propagation above about 100 MHz," Recommendation ITU-R P.2040-3, Aug. 2023. [Online]. Available: https://www.itu.int/rec/R-REC-P.2040-3-202308-S/en

[27] S. Tretyakov, *Analytical Modeling in Applied Electromagnetics*. Norwood, MA, USA: Artech House, 2003.

[28] *Building Components and Building Elements - Thermal Resistance and Thermal Transmittance - Calculation Methods*, European Standard ISO 6946:2017, Dec. 2021.

[29] V. Devanathan, "The Wiedemann-Franz law for electrical and thermal conduction in metals," *J. Chennai Acad. Sci.*, vol. 3, no. 1, pp. 1–26, 2021. [Online]. Available: https://journalcas.com/index.php/jcas/article/view/7

[30] D. Darwin, C. W. Dolan, and A. H. Nilson, *Design of Concrete Structures*, 15th ed. New York, NY, USA: McGraw-Hill Education, 2016.

[31] W. Pilkey, *Peterson's Stress Concentration Factors*. Hoboken, NJ, USA: Wiley, 2007.

[32] "1010/2017 decree of the ministry of the environment on the energy performance of new buildings," Ministry of the Environ. of Finland, Helsinki, Finland, Dec. 2017. [Online]. Available: https://ym.fi/en/the-national-building-code-of-finland